Human Molecular Genetics, 2020, Vol. 29, No. 22 3706–3716

doi: 10.1093/hmg/ddaa269
Advance Access Publication Date: 23 December 2020
General Article

GENERAL ARTICLE

RPGR isoform imbalance causes ciliary defects due to exon ORF15 mutations in X-linked retinitis pigmentosa (XLRP)

Laura Moreno-Leon[1], Emma L. West[2], Michelle O'Hara-Wright[2,†], Linjing Li[1], Rohini Nair[3], Jie He[3], Manisha Anand[1], Bhubanananda Sahu[1], Venkat Ramana Murthy Chavali[3], Alexander J. Smith[2], Robin R. Ali[2], Samuel G. Jacobson[3], Artur V. Cideciyan[3] and Hemant Khanna[1,*]

[1]Department of Ophthalmology & Visual Sciences, UMass Medical School, Worcester, MA 01655, USA, [2]Division of Molecular Therapy, UCL Institute of Ophthalmology, London EC1V 9El, UK and [3]Department of Ophthalmology, Scheie Eye Institute, University of Pennsylvania, Philadelphia, PA 19104, USA

*To whom correspondence should be addressed. Tel: 508-856-8991; Email: hemant.khanna@umassmed.edu

Downloaded from https://academic.oup.com/hmg/article/29/22/3706/6045390 by guest on 11 March 2021

Abstract

Mutations in retinitis pigmentosa GTPase regulator (*RPGR*) cause severe retinal ciliopathy, X-linked retinitis pigmentosa. Although two major alternatively spliced isoforms, RPGR$^{ex1\text{-}19}$ and RPGR^{ORF15}, are expressed, the relative importance of these isoforms in disease pathogenesis is unclear. Here, we analyzed fibroblast samples from eight patients and found that all of them form longer cilia than normal controls, albeit to different degrees. Although all mutant *RPGR*^{ORF15} messenger RNAs (mRNAs) are unstable, their steady-state levels were similar or higher than those in the control cells, suggesting there may be increased transcription. Three of the fibroblasts that had higher levels of mutant *RPGR*^{ORF15} mRNA also exhibited significantly higher levels of *RPGR*$^{ex1\text{-}19}$ mRNA. Four samples with unaltered *RPGR*$^{ex1\text{-}19}$ levels carried mutations in *RPGR*^{ORF15} that resulted in this isoform being relatively less stable. Thus, in all cases, the *RPGR*$^{ex1\text{-}19}$/*RPGR*^{ORF15} isoform ratio was increased, and this was highly correlative to the cilia extension defect. Moreover, overexpression of *RPGR*$^{ex1\text{-}19}$ (mimicking the increase in *RPGR*$^{ex1\text{-}19}$ to *RPGR*^{ORF15} isoform ratio) or *RPGR*^{ORF15} (mimicking reduction of the ratio) resulted in significantly longer or shorter cilia, respectively. Notably, the cilia length defect appears to be attributable to both the loss of the wild-type RPGR^{ORF15} protein and to the higher levels of the *RPGR*$^{ex1\text{-}19}$ isoform, indicating that the observed defect is due to the altered isoform ratios. These results suggest that maintaining the optimal *RPGR*$^{ex1\text{-}9}$ to *RPGR*^{ORF15} ratio is critical for cilia growth and that designing strategies that focus on the best ways to restore the *RPGR*$^{ex1\text{-}19}$/*RPGR*^{ORF15} ratio may lead to better therapeutic outcomes.

[†]Michelle O'Hara-Wright, http://orcid.org/0000-0002-2467-3790

Received: October 19, 2020. **Revised:** December 3, 2020. **Accepted:** December 9, 2020

© The Author(s) 2020. Published by Oxford University Press. All rights reserved. For Permissions, please email: journals.permissions@oup.com
This is an Open Access article distributed under the terms of the Creative Commons Attribution Non-Commercial License (http://creativecommons.org/licenses/by-nc/4.0/), which permits non-commercial re-use, distribution, and reproduction in any medium, provided the original work is properly cited. For commercial re-use, please contact journals.permissions@oup.com

Introduction

Primary cilia are evolutionarily conserved microtubule-based non-motile protrusions of the plasma membrane of most vertebrate cell types (1). They are nucleated from the basal bodies (mother centrioles) that dock at the apical plasma membrane in quiescent cells. The proximal region of the cilia, also called transition zone, acts as a gate. The microtubules further extend to form a distal axoneme surrounded by the ciliary membrane. The primary cilium regulates critical developmental and homeostatic signaling cascades by targeting several integral and peripheral membrane proteins as well as soluble moieties along the axoneme via a conserved mechanism termed intraflagellar transport (2,3). The trafficking is also regulated by macromolecular complexes of several proteins including retinitis pigmentosa GTPase regulator (RPGR), centrosomal protein 290 kDa (CEP290), centrosomal protein 110 kDa (CP110), Usher Syndrome proteins and Bardet Biedl Syndrome proteins (4,5). Mutations in these proteins are associated with severe developmental and homeostatic disorders collectively termed ciliopathies (6). These include Meckel–Gruber Syndrome, Joubert Syndrome, Senior–Loken Syndrome, Usher Syndrome and some forms of non-syndromic photoreceptor degenerations.

Photoreceptors (rods and cones) have a modified sensory cilium in the form of the light-sensing outer segment. The photoreceptors are one of the highly metabolically active cell types in the body. They depend upon stringently controlled proteins and lipid trafficking from their site of synthesis in the inner segment to the outer segment for light detection (7). Perturbations in the trafficking machinery due to functional deficits in ciliary proteins lead to severe photoreceptor degeneration (2,3,8). One such ciliary trafficking regulator is RPGR.

Mutations in RPGR are associated with X-linked forms of retinitis pigmentosa (RP), a debilitating blindness characterized by severe and progressive photoreceptor degeneration (9–12). *RPGR* mutations account for the majority (~70%) of X-linked retinitis pigmentosa (XLRP) cases and 12–15% of simplex RP, with no family history (12–14). In addition, *RPGR* mutations are associated with cone–rod degeneration, macular dystrophy and extraocular presentations, such as sperm abnormalities, hearing defects and primary cilia dyskinesia (15–19). Overall, *RPGR* mutations are a leading cause of blindness accounting for almost 20% of all RP cases.

The *RPGR* gene encodes two major alternatively spliced isoforms: $RPGR^{ex1\text{-}19}$ (19 exons) and $RPGR^{ORF15}$ (terminating in intron 15; exon ORF15) (20–23). The terminal exon 19 of the $RPGR^{ex1\text{-}19}$ isoform carries an isoprenylation signal involved in its localization to cilia (24,25). Exon ORF15 of the $RPGR^{ORF15}$ isoform contains purine-rich repeats that encode for a glutamic acid and glycine-rich domain (26). As majority of *RPGR* mutations are located in exon ORF15, the $RPGR^{ORF15}$ isoform has been considered the major disease-associated isoform in humans (26). The great majority of exon ORF15 mutations are predicted to prematurely truncate the $RPGR^{ORF15}$ protein.

Both RPGR isoforms are expressed throughout the body, but are particularly abundant in the retina. Previous studies have identified mouse and canine models of *RPGR* mutations and have suggested the involvement of RPGR in regulating ciliary trafficking by acting as a gatekeeper at the transition zone (27–31). Loss of RPGR alters protein trafficking to the photoreceptor outer segment, but permits its initial generation. RPGR depletion alters cilia length in cultured cell lines and fibroblasts (32). However, the effect on the ciliary defects of different $RPGR^{ORF15}$ mutations is unclear.

To investigate the effect of the human disease-causing mutations in $RPGR^{ORF15}$ on its expression and on cilia formation, we analyzed RPGR isoform expression, cilia formation and ciliary protein trafficking in patient-derived cells. Our studies unravel a new potential pathogenic mechanism of $RPGR^{ORF15}$ disease, which may assist in developing new therapies for these conditions.

Results

Ciliary defects in $RPGR^{ORF15}$-mutant fibroblasts

Given that RPGR regulates cilia length (32), we examined cilia formation in the patient and control fibroblasts. We generated primary fibroblasts from skin biopsy specimens from eight male $RPGR^{ORF15}$ patients (RPGR-1, RPGR-2, RPGR-3, RPGR-4, RPGR-5, RPGR-6, RPGR-7 and RPGR-8) with frameshift and truncation mutations in exon ORF15 (Fig. 1A and B). The patients were all from families previously confirmed to have X-linked RP due to $RPGR^{ORF15}$ mutations (33,34); their ages at skin biopsy ranged from 21 to 66 years. The patients had ophthalmoscopic features of pigmentary retinopathy, abnormal visual fields and reduced or non-detectable electroretinograms (33,34). As the control samples from the same family members could not be obtained, we included six random asymptomatic control samples without *RPGR* mutations (CTL-1, CTL-2, CTL-3, CTL-4, CTL-5 and CTL-6).

Although the control and RPGR-2 fibroblasts grew cilia in the range of 1–1.5 μm, we detected two groups of mutations with longer cilia: cilia were elongated to a range of 2.5–3.5 μm range in the RPGR-1, RPGR-3, RPGR-4 and RPGR-5 fibroblasts and to a lesser extent (1.8–2.5 μm) in RPGR-6, RPGR-7 and RPGR-8 (Fig. 2A and B). As predicted, we did not detect an effect on the number of ciliated cells.

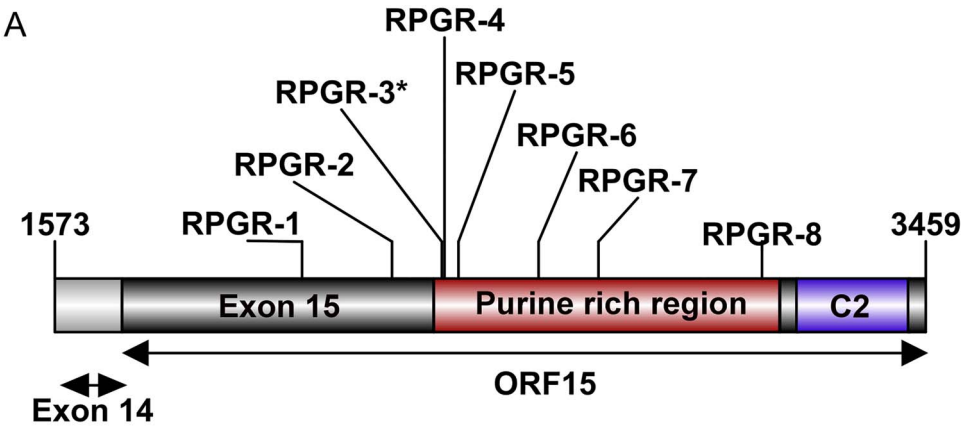
Correlation of cilia length to RPGR isoform levels in fibroblasts

We next asked whether the observed ciliary phenotype was associated with an effect of exon ORF15 mutations on RPGR expression. To this end, we performed quantitative reverse transcriptase-polymerase chain reaction (RT-PCR) analysis of the two major isoforms. We found significantly higher levels (8–10-fold) of the $RPGR^{ex1\text{-}19}$ isoform in RPGR-3, RPGR-4 and RPGR-5 fibroblasts samples when compared with the other RPGR mutants or the control fibroblasts (Fig. 3A). We also detected higher levels (2–3-fold) of the mutant $RPGR^{ORF15}$ isoform in RPGR-3, RPGR-4 and RPGR-5. Interestingly, the level of the mutant $RPGR^{ORF15}$ in RPGR-1 was significantly reduced when compared with the controls (Fig. 3B).

Given that RPGR-1, RPGR-3, RPGR-4 and RPGR-5 also formed relatively longer cilia, we tested whether there was a correlation between the $RPGR^{ex1\text{-}19}/RPGR^{ORF15}$ ratio and the cilia length. Although the RPGR-2, RPGR-6, RPGR-7, RPGR-8 and control fibroblasts showed an $RPGR^{ex1\text{-}19}/RPGR^{ORF15}$ ratio of ~10-fold, in RPGR-1, RPGR-3, RPGR-4 and RPGR-5 fibroblasts, there was an increased ratio of between 18- and 35-fold (Fig. 3C). Furthermore, we found that the length of the cilia was highly correlative to $RPGR^{ex1\text{-}19}/RPGR^{ORF15}$ ratio, with the coefficient of determination (R^2) of ~83% (Fig. 3D). Using RPGR isoform-specific antibodies (Supplementary Fig. S1A), we also detected a significant increase (18–20-fold) in the ratio of the $RPGR^{ex1\text{-}19}/RPGR^{ORF15}$ protein levels in RPGR-1, RPGR-3, RPGR-4 and RPGR-5 when compared with other RPGR mutations or controls (Supplementary Fig. S1B and C).

Downloaded from https://academic.oup.com/hmg/article/29/22/3706/6045390 by guest on 11 March 2021

A



B

Patient Code	Name	cDNA mutation	Predicted stop codon
0563	RPGR-1	c.2105_2213dup109	p.E742Gfs*64
4022	RPGR-2	c.2296_2299del GGAG	p.G766Nfs*48
5798	RPGR-3	c.2405_24067delAG	p.E802Gfs*32
5802	RPGR-4	c.2412_2418del7	p.G805Kfs*8
1338	RPGR-5	c.2442_2445delAGAG	p.G817Kfs*2
1330	RPGR-6	c.2614 G>T	p.E872*
4584	RPGR-7	c.2743 G>T	p.G915*
1533	RPGR-8	c.3092delA	p.E1031Gfs*58

Figure 1. *RPGR*^{ORF15} mutations. Schematic representation (**A**) and predicted effect of *RPGR*^{ORF15} mutations (**B**) in XLRP patients. *: optic cups of RPGR-3 were generated.

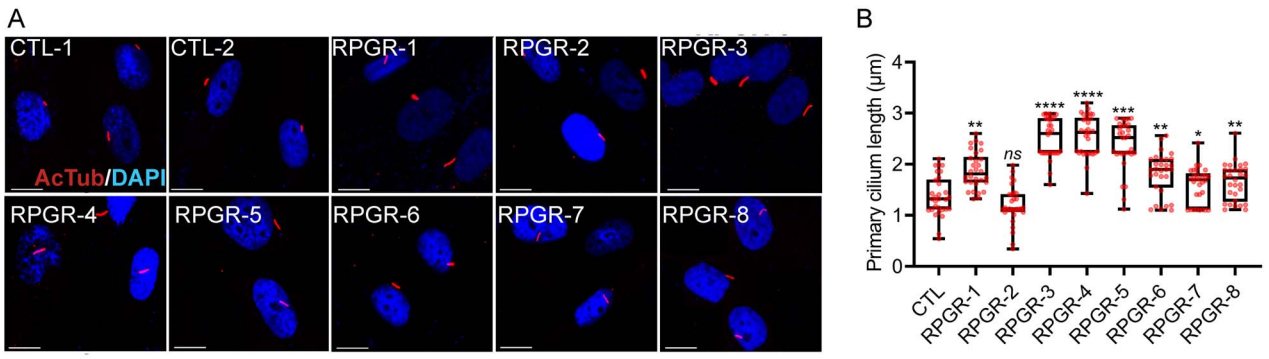


Figure 2. Ciliary defects in fibroblasts. (**A**) Control (CTL-1 and CTL-2) and mutant fibroblasts were stained for acetylated α-tubulin (red, ciliary marker) and 4′,6-diamidino-2-phenylindole (DAPI) (blue, nucleus). Scale: 5 μm. (**B**) The cilia length was quantified using the ImageJ software ($n > 100$). The CTL data represents the average cilia length of all control fibroblasts. ****$P < 0.0001$; ***$P < 0.002$; **$P < 0.01$; *$P < 0.05$.

We then checked whether such phenomenon of increased *RPGR*$^{ex1\text{-}19}$/*RPGR*^{ORF15} ratio is also conserved in retinal microenvironment. Using retinal organoids derived from reprogrammed control and RPGR-3 human-induced pluripotent stem cells (iPSCs; Supplementary Fig. S2A and B) (West *et al.* 2020, manuscript submitted), we found significant (~2.8-fold) increase in the *RPGR*$^{ex1\text{-}19}$/*RPGR*^{ORF15} ratio in the mutant sample as compared with the controls (Supplementary Fig. S2C).

These results suggest that RPGR^{ORF15} mutations tested in this study affect not only mutant *RPGR*^{ORF15} expression levels but also the *RPGR*$^{ex1\text{-}19}$ isoform levels, albeit to different extents. Although in fibroblast samples from all RPGR patients there was a positive correlation between the *RPGR*$^{ex1\text{-}19}$/*RPGR*^{ORF15} ratio and cilia length, in RPGR-1, RPGR-3, RPGR-4 and RPGR-5 samples, there were distinct effects on the *RPGR* messenger RNA (mRNA) levels. The RPGR-1 mutation results in significantly reduced mutant

Downloaded from https://academic.oup.com/hmg/article/29/22/3706/6045390 by guest on 11 March 2021

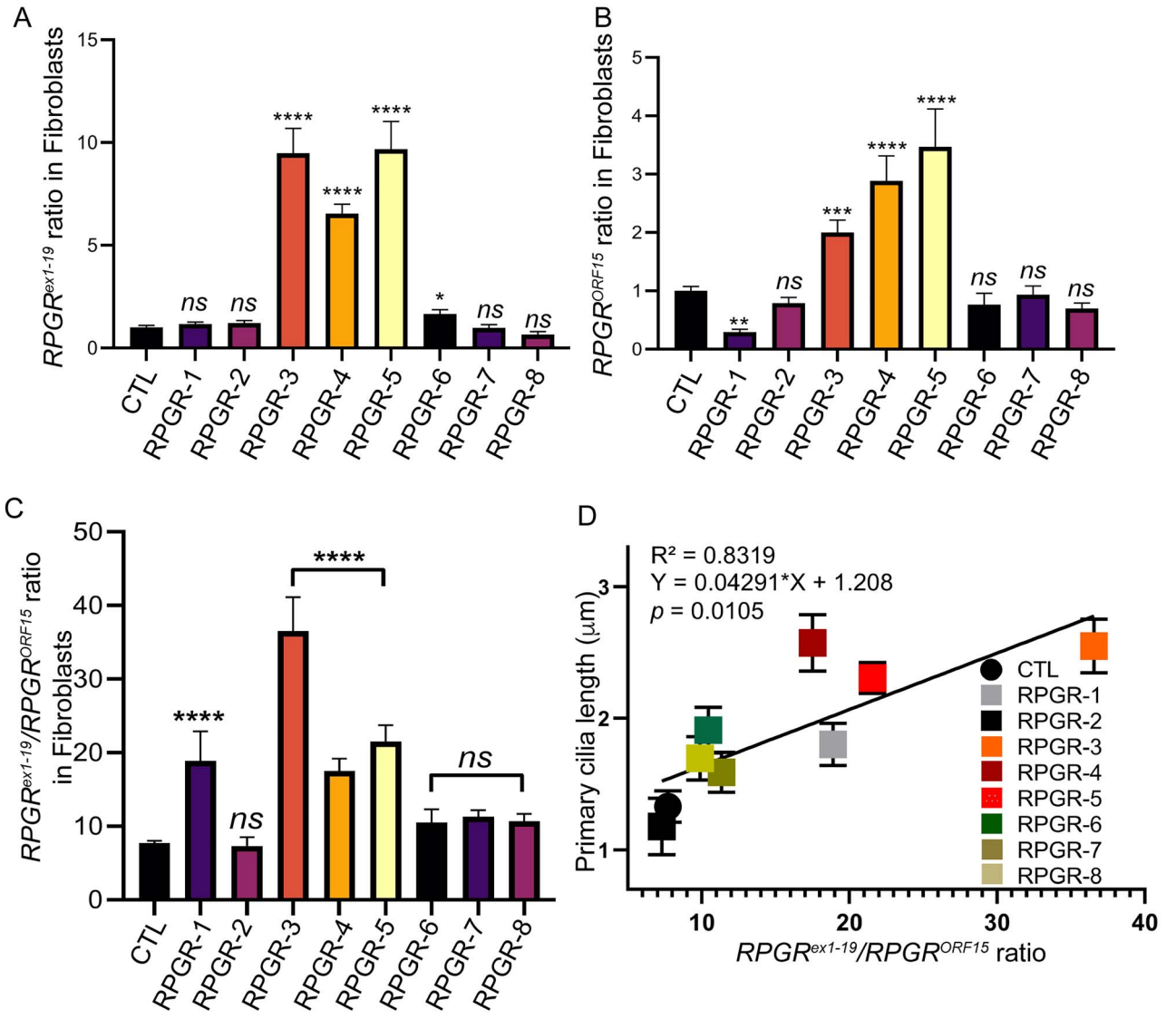


Figure 3. RPGR isoform levels in patient-derived fibroblasts. (**A, B**) $RPGR^{ex1\text{-}19}$ (A) or $RPGR^{ORF15}$ levels in the mutant fibroblasts relative to controls (CTL) were analyzed. (**C**) The ratio of $RPGR^{ex1\text{-}19}$ to $RPGR^{ORF15}$ mRNA levels was determined. RPGR-1, RPGR-3, RPGR-4 and RPGR-5 showed significantly higher ratio when compared with control (CTL) cells. ns, not significant. Data are mean ± SD from five independent experiments. (**D**) Positive correlation of the cilium length with the $RPGR^{ex1\text{-}19}/RPGR^{ORF15}$ ratio was observed. Each dot represents average cilium length of >100 cilia compared with the $RPGR^{ex1\text{-}19}/RPGR^{ORF15}$ ratio from three independent experiments. Black line shows a linear fit through the data. Inset displays the coefficient of determination (R^2) and significance (*P*-value).

$RPGR^{ORF15}$ expression, but does not affect the $RPGR^{ex1\text{-}19}$ levels. On the other hand, although the mutant $RPGR^{ORF15}$ is expressed at relatively higher levels in RPGR-3, RPGR-4 and RPGR-5 fibroblast samples, they exhibit significantly higher levels of $RPGR^{ex1\text{-}19}$. To further understand the ciliary defects, we focused on RPGR-1, RPGR-3, RPGR-4 and RPGR-5 samples. We also used RPGR-2 as it showed similar RPGR expression as the control fibroblasts.

Localization of cilia length regulators in $RPGR^{ORF15}$-mutant fibroblasts

To investigate the ciliary defect in the fibroblasts with elongated cilia, we assessed the distribution of ciliary length regulators CEP290 and distribution of glutamylated tubulin. *CEP290* mutations are a frequent cause of Leber congenital amaurosis and syndromic ciliopathies (35–37). Immunofluorescence staining of RPGR-1, RPGR-3, RPGR-4 and RPGR-5 with a previously reported CEP290 antibody demonstrated ∼50% reduction in the levels of CEP290 at the basal body (determined by the co-localization with basal body marker γ-tubulin) and concomitant increase in the cytosolic CEP290 distribution when compared with RPGR-2 or control fibroblasts (Fig. 4A and B). However, the number of CEP290-positive cells was not affected in the mutant as compared with the control fibroblasts (Fig. 4C). These results are consistent with previous studies that demonstrated longer cilia in CEP290-mutant patient fibroblasts and in *Cep290*-mutant mice (38,39) and suggest an association between the observed cilia length differences and CEP290 levels in the RPGR-mutant fibroblasts.

Tubulin polyglutamylation is a modification of the stable ciliary microtubules, which can be detected using the GT335 antibody (40,41). We found that the distribution of GT335 was altered in the $RPGR^{ORF15}$-mutant fibroblasts. Immunofluorescence analysis revealed that GT335 immunoreactivity was restricted to the

Downloaded from https://academic.oup.com/hmg/article/29/22/3706/6045390 by guest on 11 March 2021

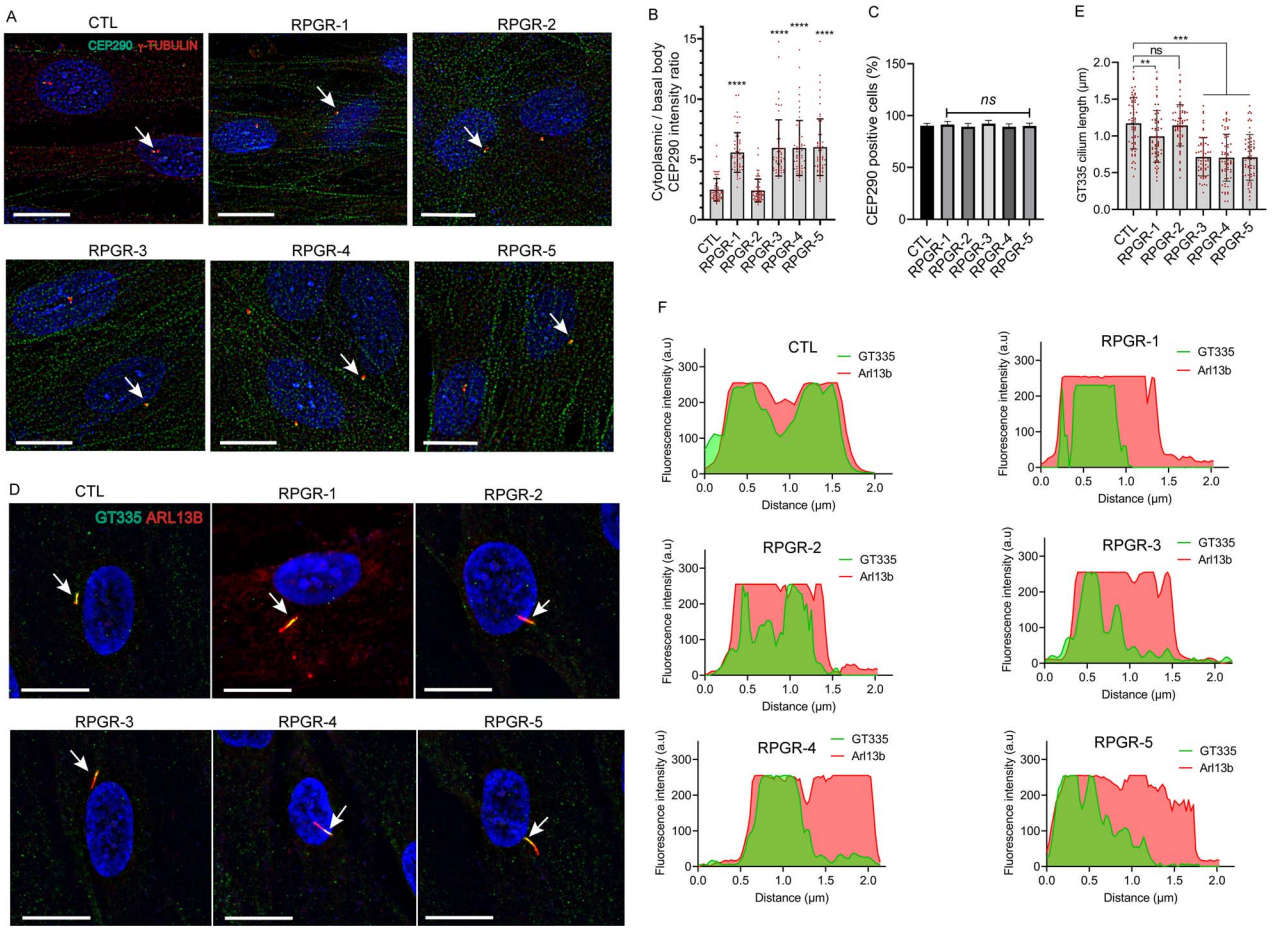


Figure 4. Distribution of ciliary markers. CEP290 (A–C) and GT335 (D–F) staining in the indicated fibroblasts was assessed. (**A**) The cells were stained with CEP290 (green) and γ-tubulin (basal body marker, red) antibodies and the ratio of the CEP290-positive signal in the cytoplasm to that at the basal body (**B**) and the number of CEP290-positive cells (**C**) were quantified using ImageJ ($n > 100$). (**D**) The cells were stained with GT335 (green, glutamylated tubulin) and ARL13B (red, cilia marker). (**E**) The distribution of GT335 (green signal intensity) along the length of the cilium when compared with ARL13B (red intensity) (distance, μm) was quantified using IMARIS software (Oxford Instruments). a.u., arbitrary units.

proximal region of the cilia in RPGR-1, RPGR-3, RPGR-4 and RPGR-5 (within ~1.0 μm) (Fig. 4D and E) when compared with RPGR-2 and the controls, in which GT335 staining is distributed across the whole cilium (Fig. 4F).

Expression of wild-type RPGR^{ORF15} in mutant fibroblasts

We then sought to determine whether the observed cilia length defects are due to the lack of the wild-type RPGR^{ORF15} protein. Transfection of the wild-type human green fluorescent protein (GFP)-RPGR^{ORF15}-encoding complementary DNA (cDNA) into RPGR-3, RPGR-4 and RPGR-5 did not completely reverse the elongated cilia phenotype when compared with cells transfected with only GFP. Although the RPGR-3, RPGR-4 and RPGR-5 fibroblasts transfected with GFP alone formed longer cilia than the CTL (control) fibroblasts, the cilia length reduced from 2.2–2.4 μm to 1.3–1.5 μm after transfection with GFP-RPGR^{ORF15} (Fig. 5A and B). RPGR-1, which had relatively modest (~1.8 μm) increase in the cilia length and *RPGR*$^{ex1\text{-}19}$/*RPGR*^{ORF15} ratio showed almost complete reversal (~1 μm) of the elongated cilia phenotype upon GFP-RPGR^{ORF15} expression. These data strongly suggest that the normal RPGR^{ORF15} protein function partly contributes to the observed cilia length changes. Samples with relatively higher *RPGR*$^{ex1\text{-}19}$/*RPGR*^{ORF15} ratio did not show complete reversal of the cilia length phenotype. Further support of this hypothesis comes from the observation that expressing RPGR^{ORF15} in the control or RPGR-2 (~20% longer cilia) cells significantly reduced the cilia length 10–20% less than the average lengths of the GFP-expressing control cells. All cells transfected with RPGR^{ORF15}-encoding cDNA overexpressed *RPGR*^{ORF15} to similar levels (4–5-fold higher) when compared with GFP-expressing control cells (Supplementary Fig. S3A) and did not alter the *RPGR*$^{ex1\text{-}19}$ levels (Supplementary Fig. S3B).

Some *RPGR*^{ORF15}-mutant isoforms are less stable

Varying mRNA levels of the RPGR isoforms could be due to the mutations affecting the purine-rich repeat region of the genomic DNA or *RPGR* mRNA stability. As some *RPGR*^{ORF15} mutations (RPGR-2, RPGR-6, RPGR-7 and RPGR-8) did not affect the isoform ratio, we concluded that the DNA architecture in the region of those mutations is not sufficient to cause the observed changes. We then tested whether the effect on RPGR isoform ratio is due to changes in its stability. We performed transcription inhibition assays using actinomycin D to assess the half-lives of the *RPGR* isoforms. Our studies revealed that the mutant *RPGR*^{ORF15} levels rapidly decrease to ~10% of the total levels within the first hour of actinomycin D treatment and are at

Downloaded from https://academic.oup.com/hmg/article/29/22/3706/6045390 by guest on 11 March 2021

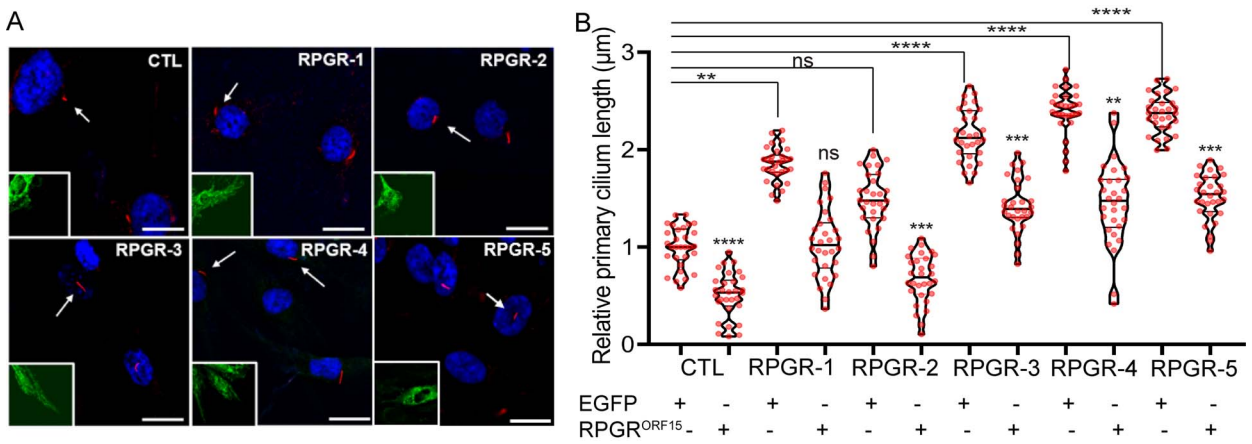


Figure 5. Effect of wild-type RPGR^{ORF15} overexpression on the cilia defect. (**A**) The fibroblasts were transiently transfected with plasmids-encoding GFP or GFP-RPGR^{ORF15} and processed for staining with the GFP (green) or acetylated α-tubulin (red, ciliary marker). Arrows point to the ciliated cells marked in the inset in green channel. The nuclei are stained with DAPI (blue). (**B**) The cilia length was quantified using ImageJ ($n > 100$). The graph shows the cilia length relative to the length of the control (CTL) fibroblasts transfected with only GFP-encoding cDNA. The statistical significance of the cilia length in the GFP or GFP-RPGR^{ORF15}-transfected mutant fibroblasts cells was determined relative to the GFP-transfected control fibroblasts. $^{**}P < 0.01$; $^{***}P < 0.0002$; $^{****}P < 0.0001$; ns, not significant. Note that the GFP-RPGR^{ORF15}-transfected RPGR-2 and CTL cells have significantly shorter cilia when compared with the GFP-transfected counterparts.

minimal levels by 4 h in RPGR-3, RPGR-4 and RPGR-5 samples. Their levels also remained significantly lower than the control at all time points. However, the rate of decline of the mutant *RPGR*^{ORF15} levels in RPGR-1 and RPGR-2 samples was overall similar to that of the control *RPGR*^{ORF15} mRNA. There was, however, a slightly faster decline of the mutant *RPGR*^{ORF15} levels in RPGR-1 and RPGR-2 at 6 and 8 h of actinomycin D treatment when compared with the control (Fig. 6A). As predicted, we did not detect a significant difference in the decay of the *RPGR*$^{ex1\text{-}19}$ mRNA in the patient fibroblasts relative to the controls (Fig. 6B). Based on these studies, we found that the half-life of the mutant *RPGR*^{ORF15} in RPGR-1 and RPGR-2 after actinomycin D treatment relative to vehicle treatment was similar to that in control fibroblasts (~2.3 and 2.2 h for RPGR-1 and RPGR-2, respectively, and 1.6 h for control) (Fig. 4C), whereas the half-life of the mutant *RPGR*^{ORF15} in RPGR-3, RPGR-4 and RPGR-5 was 0.67, 0.51 and 0.28 h, respectively. Linear regression analysis further validated that the decay kinetics of mutant *RPGR*^{ORF15} in RPGR-3, RPGR-4 and RPGR-5 does not follow a linear correlation (Fig. 6C).

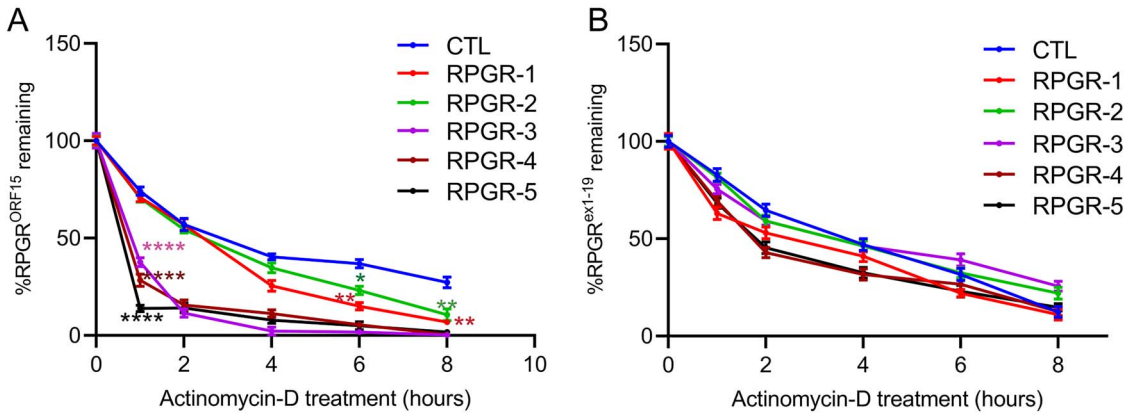
RPGR$^{ex1\text{-}19}$ knockdown in mutant fibroblasts

If RPGR^{ORF15} only partly reversed the cilia length, the increase in the *RPGR*$^{ex1\text{-}19}$ levels could also be relevant to the observed cilia elongation in the *RPGR*^{ORF15}-mutant fibroblasts. To test this, we overexpressed *RPGR*$^{ex1\text{-}19}$ in human telomerase reverse transcriptase-retinal pigmented epithelium (hTERT-RPE1) cells by transient transfection. Our analysis revealed 3–4-fold longer cilia in the *RPGR*$^{ex1\text{-}19}$ overexpressing cells as compared with the control cells (Supplementary Fig. S4A). Thus, we hypothesized that reducing the *RPGR*$^{ex1\text{-}19}$ levels will alleviate the elongated cilia phenotype. To this end, we performed small interfering ribonucleic acid (siRNA)-mediated depletion of RPGR$^{ex1\text{-}19}$. We designed three siRNAs (siRNA-1, siRNA-2 and siRNA-3) against *RPGR*$^{ex1\text{-}19}$. All siRNAs reduced the expression of RPGR$^{ex1\text{-}19}$, with maximal inhibition observed with siRNA-3 (Supplementary Fig. S4B), when compared with the levels expressed in cells transfected with a scrambled sequence control. Moreover, the siRNAs did not affect RPGR^{ORF15} levels in the fibroblasts (Supplementary Fig. S4C). Transfection of *RPGR*$^{ex1\text{-}19}$-siRNAs followed by immunofluorescence analysis in RPGR-3 and RPGR-5 revealed an almost complete reversal of the cilia elongation phenotype with the cilia length comparable with that of the scrambled siRNA-treated control fibroblasts. RPGR-4 showed ~90% reduction in cilia length compared with scrambled siRNA-treated cells (Fig. 7A and B).

Discussion

Although *RPGR*^{ORF15} gene augmentation therapy has been successful in naturally occurring canine mutations and murine models (42,43) and is currently in human clinical trials, efficacy of the treatment across the large spectrum of human exon ORF15 mutations is currently not known. We show that all eight *RPGR*^{ORF15} mutations tested here cause cilia length defects of varying extents, lead to mutant mRNA instability and four mutations lead to a significant increase in the *RPGR*$^{ex1\text{-}19}$/*RPGR*^{ORF15} ratio. Our results indicate that three out of four exon ORF15 mutations that result in an increase in the *RPGR*$^{ex1\text{-}19}$/*RPGR*^{ORF15} mRNA ratio have shorter half-life due to relatively faster mutant mRNA decay, yet have relatively higher steady-state levels of the mutant *RPGR*^{ORF15} mRNA and protein. The precise mechanism of the transcriptional complexity observed in this study is not clear. Nonetheless, these results point to transcriptional adaptation in which the unstable mRNA transcripts can result in a feedback response to increase the levels of the protein. *RPGR* transcriptional adaptation could increase the *RPGR*^{ORF15} protein levels; however, at the same time also increase *RPGR*$^{ex1\text{-}19}$ levels, as observed in this study. Such transcriptional adaptation may result from the need to compensate for the decaying mutant *RPGR*^{ORF15} transcripts (44–46); however, its relevance to retinal disease remains to be determined. We also found that the expression of wild-type RPGR^{ORF15} did not affect the elevated *RPGR*$^{ex1\text{-}19}$ levels in fibroblasts. This suggests that the mechanism of increase in the *RPGR*$^{ex1\text{-}19}$ levels is not due to the absence of the wild-type RPGR^{ORF15} and implicates the expression of the mutant ORF15 isoforms. The observed effects on cilia growth, on the

Downloaded from https://academic.oup.com/hmg/article/29/22/3706/6045390 by guest on 11 March 2021



C

Messenger RNA half-life

	CTL	RPGR-1	RPGR-2	RPGR-3	RPGR-4	RPGR-5
RPGR^{ex1-19}	1.8h	1.8h	2.2h	1.9h	1.49h	2.2h
RPGR^{ORF15}	1.6h	2.3h	2.2h	0.67h	0.51h	0.28h

Linear regression (R^2)

	CTL	RPGR-1	RPGR-2	RPGR-3	RPGR-4	RPGR-5
RPGR^{ex1-19}	0.968	0.8839	0.9176	0.8843	0.8405	0.8275
RPGR^{ORF15}	0.8418	0.9025	0.9066	0.5686	0.5464	0.4315

Figure 6. Mutant mRNA decay in *RPGR*^{ORF15} fibroblasts. Quantitative PCR analysis of *RPGR*^{ORF15} (**A**) or *RPGR*$^{ex1-19}$ (**B**) isoform was performed in fibroblasts treated with actinomycin D for indicated time. The levels of the mutant isoforms were calculated relative to the levels in the control (CTL) fibroblasts at the same time points. Statistical significance was determined by assessing the mRNA levels at each time point relative to that of the control (CTL) at the same time point. ****$P < 0.0001$; **$P < 0.01$; *$P < 0.05$. No significant changes in the degradation of *RPGR*$^{ex-19}$ mRNA were detected at the same time points (**B**). (**C**) The half-life and linear regression of the mutant *RPGR*^{ORF15} and *RPGR*$^{ex1-19}$ mRNAs was calculated by determining the time (in hours) taken by the isoforms to reduce to half the original levels.

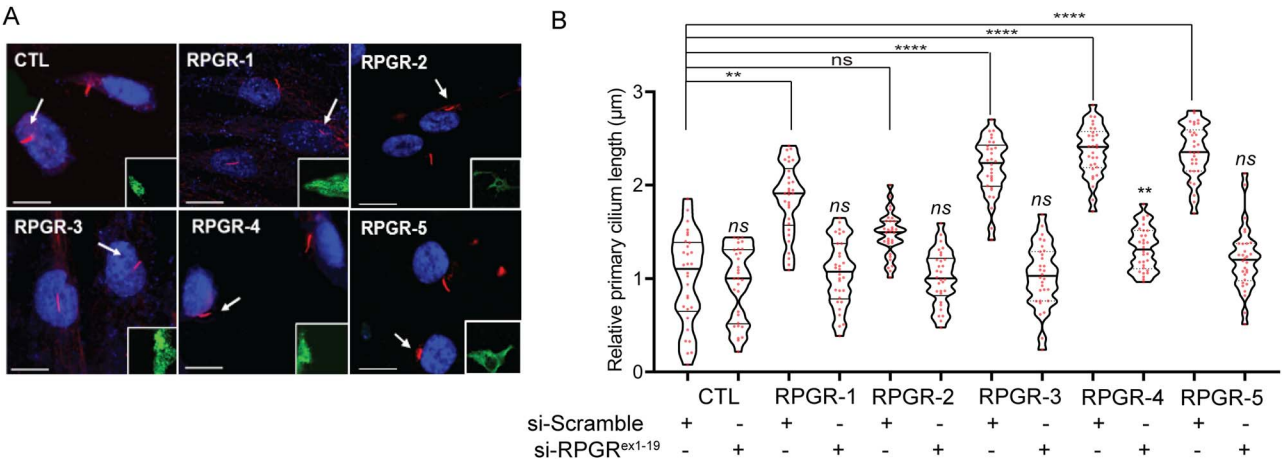


Figure 7. Effect of *RPGR*$^{ex1-19}$ knockdown on the cilia defect. (**A**) The fibroblasts were transiently transfected with RPGR-siRNA-3 or scrambled siRNA followed by GFP (green, inset) and acetylated α-tubulin staining. (**B**) The cilia length was quantified represented as the length relative to the scrambled siRNA-treated control (CTL) cells. Scale: 5 μm; ns, not significant.

other hand, seem to be due in part to the lack of the RPGR^{ORF15} protein and to the relatively increased expression of RPGR^{ex1-19}. This is because RPGR^{ORF15} overexpression or RPGR^{ex1-19} knockdown were able to partly reverse the cilia defect, with *RPGR*$^{ex1-19}$ knockdown showing better reversal of the cilia length. These results suggest that the relative levels of both RPGR isoforms are critical for optimal cilia growth. Further support of this hypothesis comes from our observation that the overexpression of *RPGR*$^{ex1-19}$ leads to longer cilia while that of *RPGR*^{ORF15} results in shorter cilia. In addition, previous studies showed that

Downloaded from https://academic.oup.com/hmg/article/29/22/3706/6045390 by guest on 11 March 2021

overexpression of *Rpgr*$^{ex1-19}$ or *RPGR*^{ORF15} in mice results in severe retinal degeneration (47,48).

What is the mechanism of cilia elongation in *RPGR*^{ORF15}-mutant samples? We found that the imbalanced *RPGR*$^{ex1-19}$/*RPGR*^{ORF15} ratio subsequently results in higher overall levels of the RPGR proteins. This could lead to increased context-dependent function of RPGR-containing protein complexes at the cilia and alteration of the gatekeeping function at the transition zone. We previously showed that RPGR regulates the composition of the ciliary outer segments of photoreceptors by affecting its ability to maintain the barrier at the transition zone (30). RPGR^{ex1-19} is also involved in regulating ciliary cargo trafficking in cultured cells as well as mouse photoreceptors (24). Moreover, both RPGR isoforms interact genetically and physically with CEP290 and this interaction is critical for photoreceptor outer segment viability and function (24). Hence, RPGR–CEP290 interaction could take place in overlapping as well as distinct complexes consisting of the different isoforms. We, therefore, propose that *RPGR*^{ORF15} mutations that perturb ratio of the two isoforms and subsequently the integrity or recruitment of the multiprotein complexes result in altered ciliary trafficking. Further studies are underway to delineate the mechanism of such effects.

Mutations in retinal ciliary proteins have been mostly associated with reduced cilia length and photoreceptor outer segment degeneration. Knockdown of *rpgr* in zebrafish or in cultured human RPE cell lines results in shorter cilia (49–52). Although the fibroblasts derived from *RPGR*^{ORF15} patients exhibited longer cilia, longer photoreceptor outer segments were not observed in iPSC-derived optic cups or in *RPGR* patients. These results could reflect cell-type specific differences in the utilization of distinct ciliary regulation pathways. Previous clinical findings and animal model studies also showed that *RPGR* mutations do not prevent the initial generation of the photoreceptor outer segments, but that they undergo progressive degeneration (28,29,31). Of note, context-dependent cilia length regulation and outer segment defects have been reported with *CEP290*-patient fibroblasts and CP110-mouse fibroblasts (39,53).

The RPGR-2, RPGR-3, RPGR-4 and RPGR-5 are similar in nature (small frameshifts), they produce profoundly different effects. These could partly be due to the location of these mutations: while the RPGR-2 mutation is located towards the 3′-region of the non-repetitive exon 15, the RPGR-3, RPGR-4 and RPGR-5 mutations lie in the 5′-region of the repetitive purine-rich region. The repetitive region of these mutations may be involved in the recognition or recruitment of mRNA decay factors or splicing effectors. On the other hand, the RPGR-1 mutation, which lies within exon 15 does not show increased *RPGR*$^{ex1-19}$ levels, yet the steady-state levels of the mutant *RPGR*^{ORF15} mRNA are significantly reduced. As the mRNA stability profile of this mutant is similar to that of the control, there may be a different mechanism underlying reduced mutant *RPGR*^{ORF15} levels. However, the resultant increase in the *RPGR*$^{ex1-19}$/*RPGR*^{ORF15} ratio indicates the similar cilia extension defect as RPGR-3, RPGR-4 and RPGR-5.

The partial effect of overexpression of *RPGR*^{ORF15} in the mutant fibroblasts on the rescue of the ciliary phenotype potentially also raises questions that they may be relevant to the ongoing clinical trials that utilize *RPGR*^{ORF15} gene augmentation strategy. These studies are based upon the rationale that the *RPGR*^{ORF15} mutations result in a complete or partial loss of function. Although our study was in progress, first results of a phase 1/2 study reported encouraging results with 7 out of 18 patients showing early improvement in visual function after *RPGR*^{ORF15} gene augmentation therapy (54). However, at least one of the patients with the mutation c.2405_2406delAG (RPGR-3) did not reveal reliable clinical improvement. Our results predict that this mutation would cause a significant disruption in the RPGR isoform ratio and abnormally longer cilia that might not be completely reversed by *RPGR*^{ORF15} overexpression. This study underscores the complexity of *RPGR* gene defects and suggests that gene therapy strategies may need to focus on ways to restore the appropriate *RPGR*$^{ex1-19}$/*RPGR*^{ORF15} ratio, taking into account the consequences of different ORF15 mutations; ORF15 overexpression may be a less effective therapeutic strategy for patients with certain *RPGR*^{ORF15} mutations.

Materials and Methods

Study approval

The skin biopsies were obtained from previously published XLRP patients and unaffected individuals after written informed consent. All procedures followed the Declaration of Helsinki and approved by the Institutional Review Board of the University of Pennsylvania and UMass Medical School.

Plasmid DNA constructs and antibodies

The plasmids-encoding human RPGR^{ORF15} or RPGR^{ex1-19} have been described (50,51). Antibody details are provided in Supplementary Table S1.

Fibroblast isolation

The biopsies were dissociated as previously described to obtain primary fibroblasts (39). Briefly, skin biopsies were washed in iodine followed by three washes in phosphate-buffered saline (Invitrogen). The sample was minced with a sharp scalpel in a culture plate and incubated with Dulbecco's-modified Eagle's medium (DMEM)/F12 (Invitrogen) supplemented with 20% fetal bovine serum (FBS) (Sigma-Aldrich, Saint-Louis, MO, USA), penicillin and streptomycin at 37°C in a humidified 5% CO_2 incubator. Ten days after harvesting, the skin was removed, and fibroblasts were passaged for storage and analysis. After dissociation, cells were grown in DMEM/F12 media containing 10% FBS at 37°C and 5% CO_2 incubator. All analyses were done in the fibroblasts at the same passage stages.

Fibroblast transfection assays

Plasmid DNA transfections was performed using FuGENE 6 (Promega) according to the manufacturer's protocol. All Dicer substrate siRNAs (RPGR^{ex1-19}, positive and negative controls, see Supplementary Table S2) were designed and purchased from Integrated DNA Technology and transfected at 20 nM using Lipofectamine RNAiMAX Reagent (Thermo Fisher Scientific), as per manufacturer's instructions. Cells were plated and transfected 24 h later at 50–70% confluency and induced to form primary cilia 24 h post-transfection by serum starvation for 24 h.

RNA extraction and quantitative reverse transcriptase-polymerase chain reaction (qRT-PCR) analysis

Total RNAs were isolated with QIAzol Lysis Reagent (Qiagen) and precipitated according to the manufacturer's instructions. Reverse transcription was performed with 1 µg of total RNAs with the SuperScript™ First-Strand Synthesis System for RT-PCR (Invitrogen). The resulting cDNA was used to perform gene expression analysis using the BioRad CFX96 qPCR instrument

Downloaded from https://academic.oup.com/hmg/article/29/22/3706/6045390 by guest on 11 March 2021

and Power SYBR Green PCR Master Mix (Thermo Fisher Scientific). The isoform-specific quantitative PCR (qPCR) primers are described in Supplementary Table S2.

RNA stability assay

Messenger RNA decay after transcriptional inhibition with actinomycin D treatment was performed as previously described (55). Briefly, the fibroblasts were plated at 50% confluency in six-well plates; 24 h later, cells were treated with 10 µg/ml actinomycin D (Sigma-Aldrich) in DMEM/F12 media for 1, 2, 4, 6 and 8 h. Total mRNA was extracted and subjected to RT-qPCR. Experiments were conducted in triplicates and mRNA decay rate was determined by non-linear regression curve fitting (one-phase decay) using GraphPad Prism Software.

Immunoblotting

The cells were lyzed on ice in Pierce RIPA Buffer (Thermo Scientific) containing Halt™ Protease Inhibitor Cocktail (100X, Thermo Fisher). Lysates were sonicated and centrifugated at 12 000*g* for 15 min. Supernatants were quantified and 20 µg of total protein lysate was incubated for 5 min at 95°C with Laemmli sample buffer. Proteins were separated on a 4–20% Mini-PROTEAN® TGX™ Precast Protein Gel (BioRad) and transferred to a nitrocellulose membrane (BioRad). The blots were processed using LI-COR western blotting instructions and blocking, and primary and secondary antibodies solutions were prepared in Intercept Blocking buffer (LI-COR). Primary antibodies were incubated overnight at 4°C and secondary antibodies were incubated at room temperature for 2 h (see supplementary table for antibodies details and dilution information). Protein expression was detected using LI-COR Odyssey Fc detection system and quantified with Image Studio Lite quantification software (LI-COR).

Immunofluorescence, microscopy and co-localization analysis

The primary fibroblasts were plated on coverslips (AmScope CS-R18-100) and fixed in pre-chilled 100% methanol at −20°C for 5 min or in 4% paraformaldehyde/1X Dulbecco's phosphate-buffered saline (DPBS; potassium chloride 0.2 g/L, potassium dihydrogen phosphate 0.2 g/L, sodium chloride 8 g/L and disodium hydrogen phosphate 1.15 g/L) for 10 min, washed three times in DPBS and blocked in DPBS containing 5% normal goat serum and 0.5% Triton X-100 for 1 h. Primary antibody solution was prepared in blocking solution and incubated overnight at 4°C. After washing in DPBS, cells were incubated in blocking solution containing Alexa-488-conjugated and Alexa-546-conjugated (Invitrogen) for 1 h. Finally, cells were washed in DPBS and incubated for 5 min with DAPI for nuclear staining. Coverslips were mounted with Antifade Mounting Media (Vectashield) and all images were visualized over 63× objective using a Leica DM6 Thunder microscope with a 16 bit monochrome camera.

Cilia length was measured on single z-stacks using the ImageJ software and line and measure tool. An average of 15 cilia were measured in at least five different coverslip area using acetylated tubulin or ADP-ribosylation factor like 13B (ARL13B) ciliary markers. The IMARIS platform was used to process the two channel intensities simultaneously and to measure the degree of overlap of the two channels. After setting intensity threshold, the basal body marker γ-tubulin was used to define a region of interest and a co-localization channel was built on different z-stacks to obtain the percentage of co-localized signal and intensity. When needed, adjacent optical sections were merged in the z-axis to form a projected image (ImageJ). Co-localization value was plotted using the GraphPad Prism software.

Statistics

All data are presented as means ± standard derivation from the mean. Two groups comparison was analyzed by Student's *t*-tests using the Prism GraphPad software. Multiple groups comparison was performed with one-way analysis of variance. Differences between groups were considered statistically significant if $P < 0.05$. The statistical significance is denoted with asterisks ($^{*}P < 0.05$; $^{**}P < 0.01$; $^{***}P < 0.005$; $^{****}P < 0.001$).

Supplementary Material

Supplementary Material is available at *HMG* online.

Funding

National Institutes of Health (EY022372 and EY029050 to H.K., EY028273 and P30EY01583 to V.R.M.C. and EY017549 to S.G.J. and A.V.C.); Medical Research Council UK (MR/T002735/1, MR/J004553/1); European Research Council (323147-STEMRD); Retina UK (GR576 to R.R.A.); Research to Prevent Blindness Unrestricted Grant Funds to Scheie Eye Institute.

Acknowledgement

The authors thank the patients and families who participated in these studies. The authors also thank Dr Gregory Pazour (UMMS) for providing the fibroblasts of control individuals and Dr Michael Volkert (UMMS) for critical inputs and suggestions on this project.

Conflict of Interest statement. None declared.

References

1. Singla, V. and Reiter, J.F. (2006) The primary cilium as the cell's antenna: signaling at a sensory organelle. *Science*, **313**, 629–633.
2. Pazour, G.J. and Rosenbaum, J.L. (2002) Intraflagellar transport and cilia-dependent diseases. *Trends Cell Biol.*, **12**, 551–555.
3. Baker, S.A., Freeman, K., Luby-Phelps, K., Pazour, G.J. and Besharse, J.C. (2003) IFT20 links kinesin II with a mammalian intraflagellar transport complex that is conserved in motile flagella and sensory cilia. *J. Biol. Chem.*, **278**, 34211–34218.
4. Khanna, H. (2015) Photoreceptor sensory cilium: traversing the ciliary gate. *Cell*, **4**, 674–686.
5. Chen, H.Y., Kelley, R.A., Li, T. and Swaroop, A. (2020) Primary cilia biogenesis and associated retinal ciliopathies. *Semin. Cell Dev. Biol.* 19, 30167–30173.
6. Badano, J.L., Leitch, C.C., Ansley, S.J., May-Simera, H., Lawson, S., Lewis, R.A., Beales, P.L., Dietz, H.C., Fisher, S. and Katsanis, N. (2006) Dissection of epistasis in oligogenic Bardet-Biedl syndrome. *Nature*, **439**, 326–330.
7. Besharse, J.C. (1986) *The Retina: A Model for Cell Biological Studies Part I*. Academic, New York.
8. Arts, H.H., Doherty, D., van Beersum, S.E., Parisi, M.A., Letteboer, S.J., Gorden, N.T., Peters, T.A., Marker, T., Voesenek, K., Kartono, A. *et al.* (2007) Mutations in the gene encoding the

Downloaded from https://academic.oup.com/hmg/article/29/22/3706/6045390 by guest on 11 March 2021

basal body protein RPGRIP1L, a nephrocystin-4 interactor, cause Joubert syndrome. *Nat. Genet.*, **39**, 882–888.
9. Berson, E.L. (1996) Retinitis pigmentosa: unfolding its mystery. *Proc. Natl. Acad. Sci. U. S. A.*, **93**, 4526–4528.
10. Bird, A.C. (1987) Clinical investigation of retinitis pigmentosa. *Prog. Clin. Biol. Res.*, **247**, 3–20.
11. Hanany, M., Rivolta, C. and Sharon, D. (2020) Worldwide carrier frequency and genetic prevalence of autosomal recessive inherited retinal diseases. *Proc. Natl. Acad. Sci. U. S. A.*, **117**, 2710–2716.
12. Churchill, J.D., Bowne, S.J., Sullivan, L.S., Lewis, R.A., Wheaton, D.K., Birch, D.G., Branham, K.E., Heckenlively, J.R. and Daiger, S.P. (2013) Mutations in the X-linked retinitis pigmentosa genes RPGR and RP2 found in 8.5% of families with a provisional diagnosis of autosomal dominant retinitis pigmentosa. *Invest. Ophthalmol. Vis. Sci.*, **54**, 1411–1416.
13. Breuer, D.K., Yashar, B.M., Filippova, E., Hiriyanna, S., Lyons, R.H., Mears, A.J., Asaye, B., Acar, C., Vervoort, R., Wright, A.F. *et al.* (2002) A comprehensive mutation analysis of RP2 and RPGR in a North American cohort of families with X-linked retinitis pigmentosa. *Am. J. Hum. Genet.*, **70**, 1545–1554.
14. Sharon, D., Sandberg, M.A., Rabe, V.W., Stillberger, M., Dryja, T.P. and Berson, E.L. (2003) RP2 and RPGR mutations and clinical correlations in patients with X-linked retinitis pigmentosa. *Am. J. Hum. Genet.*, **73**, 1131–1146.
15. Ayyagari, R., Demirci, F.Y., Liu, J., Bingham, E.L., Stringham, H., Kakuk, L.E., Boehnke, M., Gorin, M.B., Richards, J.E. and Sieving, P.A. (2002) X-linked recessive atrophic macular degeneration from RPGR mutation. *Genomics*, **80**, 166–171.
16. Hunter, D.G., Fishman, G.A. and Kretzer, F.L. (1988) Abnormal axonemes in X-linked retinitis pigmentosa. *Arch. Ophthalmol.*, **106**, 362–368.
17. Iannaccone, A., Breuer, D.K., Wang, X.F., Kuo, S.F., Normando, E.M., Filippova, E., Baldi, A., Hiriyanna, S., MacDonald, C.B., Baldi, F. *et al.* (2003) Clinical and immunohistochemical evidence for an X linked retinitis pigmentosa syndrome with recurrent infections and hearing loss in association with an RPGR mutation. *J. Med. Genet.*, **40**, e118.
18. Koenekoop, R.K., Loyer, M., Hand, C.K., Al Mahdi, H., Dembinska, O., Beneish, R., Racine, J. and Rouleau, G.A. (2003) Novel RPGR mutations with distinct retinitis pigmentosa phenotypes in French-Canadian families. *Am. J. Ophthalmol.*, **136**, 678–687.
19. Bukowy-Bieryllo, Z., Zietkiewicz, E., Loges, N.T., Wittmer, M., Geremek, M., Olbrich, H., Fliegauf, M., Voelkel, K., Rutkiewicz, E., Rutland, J. *et al.* (2013) RPGR mutations might cause reduced orientation of respiratory cilia. *Pediatr. Pulmonol.*, **48**, 352–363.
20. Meindl, A., Dry, K., Herrmann, K., Manson, F., Ciccodicola, A., Edgar, A., Carvalho, M.R., Achatz, H., Hellebrand, H., Lennon, A. *et al.* (1996) A gene (RPGR) with homology to the RCC1 guanine nucleotide exchange factor is mutated in X-linked retinitis pigmentosa (RP3). *Nat. Genet.*, **13**, 35–42.
21. Roepman, R., van Duijnhoven, G., Rosenberg, T., Pinckers, A.J., Bleeker-Wagemakers, L.M., Bergen, A.A., Post, J., Beck, A., Reinhardt, R., Ropers, H.H. *et al.* (1996) Positional cloning of the gene for X-linked retinitis pigmentosa 3: homology with the guanine-nucleotide-exchange factor RCC1. *Hum. Mol. Genet.*, **5**, 1035–1041.
22. Mears, A.J., Hiriyanna, S., Vervoort, R., Yashar, B., Gieser, L., Fahrner, S., Daiger, S.P., Heckenlively, J.R., Sieving, P.A., Wright, A.F. and Swaroop, A. (2000) Remapping of the RP15 locus for X-linked cone-rod degeneration to Xp11.4-p21.1, and identification of a de novo insertion in the RPGR exon ORF15. *Am. J. Hum. Genet.*, **67**, 1000–1003.
23. He, S., Parapuram, S.K., Hurd, T.W., Behnam, B., Margolis, B., Swaroop, A. and Khanna, H. (2008) Retinitis pigmentosa GTPase regulator (RPGR) protein isoforms in mammalian retina: insights into X-linked retinitis pigmentosa and associated ciliopathies. *Vision Res.*, **48**, 366–376.
24. Rao, K.N., Zhang, W., Li, L., Ronquillo, C., Baehr, W. and Khanna, H. (2016) Ciliopathy-associated protein CEP290 modifies the severity of retinal degeneration due to loss of RPGR. *Hum. Mol. Genet.*, **25**, 2005–2012.
25. Lee, J.J. and Seo, S. (2015) PDE6D binds to the C-terminus of RPGR in a prenylation-dependent manner. *EMBO Rep.* 16, 1581–1582.
26. Vervoort, R. and Wright, A.F. (2002) Mutations of RPGR in X-linked retinitis pigmentosa (RP3). *Hum. Mutat.*, **19**, 486–500.
27. Hosch, J., Lorenz, B. and Stieger, K. (2011) RPGR: role in the photoreceptor cilium, human retinal disease, and gene therapy. *Ophthalmic Genet.*, **32**, 1–11.
28. Schlegel, J., Hoffmann, J., Roll, D., Muller, B., Gunther, S., Zhang, W., Janise, A., Vossing, C., Fuhler, B., Neidhardt, J. *et al.* (2019) Toward genome editing in X-linked RP-development of a mouse model with specific treatment relevant features. *Transl. Res.*, **203**, 57–72.
29. Zhang, Q., Acland, G.M., Wu, W.X., Johnson, J.L., Pearce-Kelling, S., Tulloch, B., Vervoort, R., Wright, A.F. and Aguirre, G.D. (2002) Different RPGR exon ORF15 mutations in Canids provide insights into photoreceptor cell degeneration. *Hum. Mol. Genet.*, **11**, 993–1003.
30. Rao, K.N., Li, L., Anand, M. and Khanna, H. (2015) Ablation of retinal ciliopathy protein RPGR results in altered photoreceptor ciliary composition. *Sci. Rep.*, **5**, 11137.
31. Hong, D.H., Pawlyk, B.S., Shang, J., Sandberg, M.A., Berson, E.L. and Li, T. (2000) A retinitis pigmentosa GTPase regulator (RPGR)-deficient mouse model for X-linked retinitis pigmentosa (RP3). *Proc. Natl. Acad. Sci. U. S. A.*, **97**, 3649–3654.
32. Rao, K.N., Zhang, W., Li, L., Anand, M. and Khanna, H. (2016) Prenylated retinal ciliopathy protein RPGR interacts with PDE6delta and regulates ciliary localization of Joubert syndrome-associated protein INPP5E. *Hum. Mol. Genet.*, **25**, 4533–4545.
33. Charng, J., Cideciyan, A.V., Jacobson, S.G., Sumaroka, A., Schwartz, S.B., Swider, M., Roman, A.J., Sheplock, R., Anand, M., Peden, M.C. *et al.* (2016) Variegated yet non-random rod and cone photoreceptor disease patterns in RPGR-ORF15-associated retinal degeneration. *Hum. Mol. Genet.*, **25**, 5444–5459.
34. Huang, W.C., Wright, A.F., Roman, A.J., Cideciyan, A.V., Manson, F.D., Gewaily, D.Y., Schwartz, S.B., Sadigh, S., Limberis, M.P., Bell, P. *et al.* (2012) RPGR-associated retinal degeneration in human X-linked RP and a murine model. *Invest. Ophthalmol. Vis. Sci.*, **53**, 5594–5608.
35. den Hollander, A.I., Koenekoop, R.K., Yzer, S., Lopez, I., Arends, M.L., Voesenek, K.E., Zonneveld, M.N., Strom, T.M., Meitinger, T., Brunner, H.G. *et al.* (2006) Mutations in the CEP290 (NPHP6) gene are a frequent cause of Leber congenital amaurosis. *Am. J. Hum. Genet.*, **79**, 556–561.
36. den Hollander, A.I., Roepman, R., Koenekoop, R.K. and Cremers, F.P. (2008) Leber congenital amaurosis: genes, proteins and disease mechanisms. *Prog. Retin. Eye Res.*, **27**, 391–419.
37. Sayer, J.A., Otto, E.A., O'Toole, J.F., Nurnberg, G., Kennedy, M.A., Becker, C., Hennies, H.C., Helou, J., Attanasio, M., Fausett, B.V. *et al.* (2006) The centrosomal protein

Downloaded from https://academic.oup.com/hmg/article/29/22/3706/6045390 by guest on 11 March 2021

nephrocystin-6 is mutated in Joubert syndrome and activates transcription factor ATF4. *Nat. Genet.*, **38**, 674–681.
38. Rachel, R.A., Yamamoto, E.A., Dewanjee, M.K., May-Simera, H.L., Sergeev, Y.V., Hackett, A.N., Pohida, K., Munasinghe, J., Gotoh, N., Wickstead, B. *et al.* (2015) CEP290 alleles in mice disrupt tissue-specific cilia biogenesis and recapitulate features of syndromic ciliopathies. *Hum. Mol. Genet.*, **24**, 3775–3791.
39. Shimada, H., Lu, Q., Insinna-Kettenhofen, C., Nagashima, K., English, M.A., Semler, E.M., Mahgerefteh, J., Cideciyan, A.V., Li, T., Brooks, B.P. *et al.* (2017) In vitro modeling using ciliopathy-patient-derived cells reveals distinct cilia dysfunctions caused by CEP290 mutations. *Cell Rep.*, **20**, 384–396.
40. van Dijk, J., Miro, J., Strub, J.M., Lacroix, B., van Dorsselaer, A., Edde, B. and Janke, C. (2008) Polyglutamylation is a post-translational modification with a broad range of substrates. *J. Biol. Chem.*, **283**, 3915–3922.
41. Rao, K.N., Anand, M. and Khanna, H. (2016) The carboxyl terminal mutational hotspot of the ciliary disease protein RPGRORF15 (retinitis pigmentosa GTPase regulator) is glutamylated in vivo. *Biol. Open*, **5**, 424–428.
42. Beltran, W.A., Cideciyan, A.V., Lewin, A.S., Iwabe, S., Khanna, H., Sumaroka, A., Chiodo, V.A., Fajardo, D.S., Roman, A.J., Deng, W.T. *et al.* (2012) Gene therapy rescues photoreceptor blindness in dogs and paves the way for treating human X-linked retinitis pigmentosa. *Proc. Natl. Acad. Sci. U. S. A.*, **109**, 2132–2137.
43. Pawlyk, B.S., Bulgakov, O.V., Sun, X., Adamian, M., Shu, X., Smith, A.J., Berson, E.L., Ali, R.R., Khani, S., Wright, A.F. *et al.* (2015) Photoreceptor rescue by an abbreviated human RPGR gene in a murine model of X-linked retinitis pigmentosa. *Gene Ther.* 23, 196–204.
44. El-Brolosy, M.A., Kontarakis, Z., Rossi, A., Kuenne, C., Gunther, S., Fukuda, N., Kikhi, K., Boezio, G.L.M., Takacs, C.M., Lai, S.L. *et al.* (2019) Genetic compensation triggered by mutant mRNA degradation. *Nature*, **568**, 193–197.
45. Rossi, A., Kontarakis, Z., Gerri, C., Nolte, H., Holper, S., Kruger, M. and Stainier, D.Y. (2015) Genetic compensation induced by deleterious mutations but not gene knockdowns. *Nature*, **524**, 230–233.
46. Tautz, D. (2000) A genetic uncertainty problem. *Trends Genet.*, **16**, 475–477.
47. Hong, D.H., Pawlyk, B.S., Adamian, M. and Li, T. (2004) Dominant, gain-of-function mutant produced by truncation of RPGR. *Invest. Ophthalmol. Vis. Sci.*, **45**, 36–41.
48. Wright, R.N., Hong, D.H. and Perkins, B. (2011) Misexpression of the constitutive Rpgr(ex1-19) variant leads to severe photoreceptor degeneration. *Invest. Ophthalmol. Vis. Sci.*, **52**, 5189–5201.
49. Gakovic, M., Shu, X., Kasioulis, I., Carpanini, S., Moraga, I. and Wright, A.F. (2011) The role of RPGR in cilia formation and actin stability. *Hum. Mol. Genet.*, **20**, 4840–4850.
50. Ghosh, A.K., Murga-Zamalloa, C.A., Chan, L., Hitchcock, P.F., Swaroop, A. and Khanna, H. (2010) Human retinopathy-associated ciliary protein retinitis pigmentosa GTPase regulator mediates cilia-dependent vertebrate development. *Hum. Mol. Genet.*, **19**, 90–98.
51. Murga-Zamalloa, C.A., Atkins, S.J., Peranen, J., Swaroop, A. and Khanna, H. (2010) Interaction of retinitis pigmentosa GTPase regulator (RPGR) with RAB8A GTPase: implications for cilia dysfunction and photoreceptor degeneration. *Hum. Mol. Genet.*, **19**, 3591–3598.
52. Shu, X., Zeng, Z., Gautier, P., Lennon, A., Gakovic, M., Patton, E.E. and Wright, A.F. (2010) Zebrafish Rpgr is required for normal retinal development and plays a role in dynein-based retrograde transport processes. *Hum. Mol. Genet.*, **19**, 657–670.
53. Yadav, S.P., Sharma, N.K., Liu, C., Dong, L., Li, T. and Swaroop, A. (2016) Centrosomal protein CP110 controls maturation of the mother centriole during cilia biogenesis. *Development*, **143**, 1491–1501.
54. Cehajic-Kapetanovic, J., Xue, K., Martinez-Fernandez de la Camara, C., Nanda, A., Davies, A., Wood, L.J., Salvetti, A.P., Fischer, M.D., Aylward, J.W., Barnard, A.R. *et al.* (2020) Initial results from a first-in-human gene therapy trial on X-linked retinitis pigmentosa caused by mutations in RPGR. *Nat. Med.*, **26**, 354–359.
55. Ratnadiwakara, M. and Änkö, M.-L. (2018) mRNA stability assay using transcription inhibition by actinomycin D in mouse pluripotent stem cells. *Bio-Protocol*, **8**, e3072.

Downloaded from https://academic.oup.com/hmg/article/29/22/3706/6045390 by guest on 11 March 2021